Review

Recent Developments on Biomineralization for Erosion Control

Shan Liu , Changrui Dong , Yonggiang Zhu , Zichun Wang , Yujie Li * , Guohui Feng

Posted Date: 19 May 2025

doi: 10.20944/preprints202505.1387.v1

Keywords: microbially induced calcium carbonate precipitation (MICP); sustainability; erosion control; biomineralization; ocean engineering; scour protection

 doi:10.20944/preprints202505.1387.v1

Review

Recent Developments on Biomineralization for Erosion Control

Shan Liu [1], Changrui Dong [2], Yongqiang Zhu [2], Zichun Wang [2],Yujie Li [3,*] and Guohui Feng [4]

[1] Zhejiang Tongji Vocational College of Science and Technology, Hangzhou 311231, China
[2] Zhejiang Province Key Laboratory of Offshore Geotechnics and Material, College of Civil Engineering and Architecture, Zhejiang University, Hangzhou 310058, China
[3] Ocean College, Zhejiang University, Zhoushan, 316021, China
[4] Department of Civil Engineering, Hangzhou City University, Hangzhou, 310015, China
* Correspondence: liyujies@zju.edu.cn

Abstract: Erosion pose significant threats to infrastructures and ecosystems, exacerbated by climate change driven sea-level rise and intensified wave actions. Microbially induced calcium carbonate precipitation (MICP) has emerged as a promising, sustainable, and eco-friendly solution for erosion mitigation. This review synthesizes recent advancements in optimizing biomineralization efficiency, multi-scale erosion control, and field-scale MICP implementations. Key findings include: (1) Kinetic analysis of Ca^{2+} conversion confirmed complete ion utilization within 24 hours under optimized PA concentration (3%), resulting in a compressive strength of 2.76 MPa after five treatment cycles. (2) The erosion resistance of coastal soil was investigated through erosion function apparatus tests, model tests and field applications. Field validations in Ahoskie and Sanya demonstrated the efficacy of MICP in coastal erosion control through tailored delivery systems and environmental adaptations. (3) MICP coupled with polyvinyl alcohol (PVA) was shown to effectively mitigate local scour around monopile. Experimental studies revealed that MICP treatments (2-4 cycles) reduced maximum scour depth by 84-100% under unidirectional currents. MICP coupled with PVA outperforms conventional methods. (4) Numerical simulations revealed MICP enhanced seabed stability by increasing vertical effective stress and reducing pore pressure. Comparative analysis demonstrates that while the destabilization depth of untreated seabed sediments exhibits a linear correlation with wave height increments, MICP-treated seabed formations maintain exceptional stability through cohesion-enhancing properties, even when subjected to progressively intensified wave forces. This work establishes a foundational framework for advancing biomineralization technologies in erosion control, with significant implications for developing sustainable, nature-based solutions in ocean geotechnical engineering.

Keywords: microbially induced calcium carbonate precipitation (MICP); sustainability; erosion control; biomineralization; ocean engineering; scour protection

1. Introduction

In ocean geotechnical engineering, erosion is an inevitable problem, the most typical of which include coastal erosion, local scour around piles, and increased erosion caused by seabed liquefaction. Coastal erosion, driven by sediment transport imbalances under wave and flow dynamics, poses a global threat to land resources and infrastructures. It has been reported that at least 70% of sandy slopes around the world have retreated [1]. In the USA, about 86% of the beaches along the East Coast have experienced erosion over the past century [2]. Between 1984 and 2015, 28,000 square kilometers of land worldwide were lost to erosion globally, with stretches of shoreline on England's east coast expected to retreat by 20 meters in the coming years. Presently, the total coastal area lost in Europe due to erosion is estimated to be about 15 km^2 per year. The annual cost of mitigation measures is

 doi:10.20944/preprints202505.1387.v1

estimated to be about 3 billion euros per year. As shown in Figure 1, mid-century projections under RCP 4.5 and RCP 8.5 scenarios indicate global mean long-term shoreline displacements (dxshore, LT) with 90% confidence intervals spanning erosion-dominated ranges of -78.1 to -1.1 m and -98.1 to 0.3 m, respectively. In general, a high percentage of world coastlines experience issues related to coastal erosion [3,4], the coastal erosion problem becomes much more significant, as coastlines are the ideal place for human concentrations, and the development of different productive activities [5]. In addition, under the action of current, the horseshoe vortex and wake vortex will appear around the pile foundation because of hindering effect. The horseshoe vortex interacts strongly with the seabed soil, increasing the local shear stress, causing the soil particles to start and migration, while the wake vortex forms a negative pressure zone, making it easier for the soil particles below to start and migration [6–11]. Results of Raudkivi and Ettema (1983) show that the scour depth under static bed condition is related to the median particle size, particle size distribution, the ratio of water depth to pile diameter, and the ratio of water depth to soil particle size, the ultimate equilibrium scour depth given is about 2.3 times the pile diameter [12]. For living bed condition, many researchers believe that the ultimate equilibrium scour depth can be taken as 1.3 times the pile diameter [13]. Scour will reduce the buried depth of the pile foundation, increase the eccentricity of the horizontal load, and affect the stress history of the remaining soil, greatly weakening the horizontal bearing capacity of the pile foundation [15,16]. The wave-induced excess pore pressure response of the seabed will also cause the seabed soil to completely or partially liquefaction, resulting in the weakening or even loss of bearing capacity. Wave induced seabed liquefaction includes transient liquefaction and residual liquefaction. The transient pore pressure response is the periodic pulsation of pore water pressure in seabed caused by cyclic wave actions. In the trough, the transient pore pressure has an upward pressure gradient, which generates seepage in the soil. When the seepage force is greater than the weight of the soil particles, transient liquefaction will occur in the soil [17–22]. The cumulative pore pressure response, also known as the residual pore pressure response, is the effect of the growth of pore water pressure over time due to soil skeleton compression and poor drainage under cyclic wave pressure. Under the continuous actions of wave, the residual pore pressure of the soil may continue to rise. When the excess pore pressure exceeds the effective stress of the soil overlying, the cumulative liquefaction occurs [23–26].

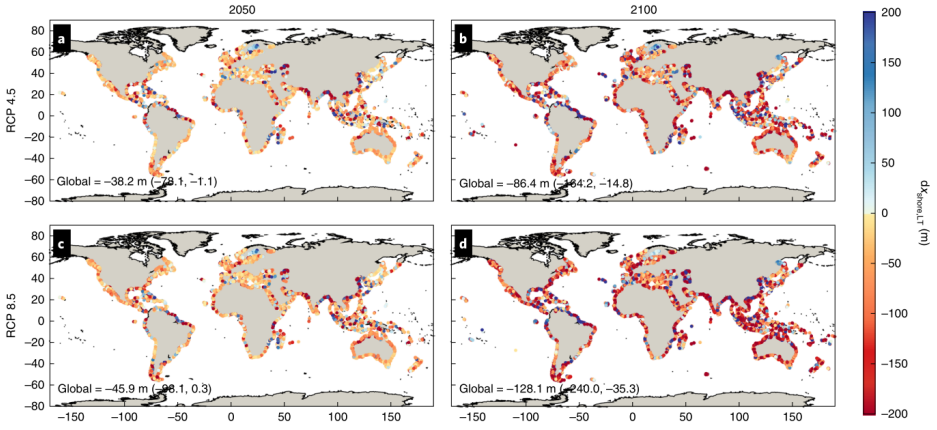

Figure 1. Projected shoreline changes by the years 2050 (a, c) and 2100 (b, d) under RCP 4.5 (a, b) and RCP 8.5 (c, d). Values represent the median change and positive/negative values, respectively, express accretion/erosion in metres, relative to 2010 [27].

Billions of dollars have been invested in erosion or liquefaction defences in ocean engineering, including riprap, seawalls, breakwaters, fluidized solid soil, beach nourishment, and mangrove afforestation [28–31]. While seawalls and breakwaters effectively reduce the loss of coastal soil and offer long service life, they can cause secondary erosion. The construction of these structures requires

 doi:10.20944/preprints202505.1387.v1

significant amounts of concrete, which not only causes a large amount of carbon emissions, but also forms a permanent cementation on the beach, threatening the normal growth and activities of organisms. Riprap and beach nourishment, while avoiding environmental pollution, require ongoing maintenance. The long plant growth cycle of mangrove afforestation also needs to be considered, although this technology comes from nature. In general, these conventional approaches, while protective, can be costly and environmentally damaging when considering material, energy, time, cost, and environmental impact. Therefore, it is very meaningful to seek sustainable and environmentally friendly methods to prevent coastal erosion of sandy slopes and liquefaction of seabed.

Inspired by the unique process of soil diagenesis under the intervention of bacteria, Microbially induced calcium carbonate precipitation (MICP) offers an innovative approach to improve sand engineering characteristics while simultaneously affording the potential to achieve significant environmental benefits when compared to other business-as-usual reinforcement techniques. MICP involves urease-producing bacteria, such as Sporosarcina pasteurii, to hydrolyze urea and produce calcium carbonate in the presence of calcium ions. The generated calcium carbonate ($CaCO_3$) improves the strength, stiffness and erosion resistance of the sand in the form of particle bonding, pore plugging and particle coating [32]. MICP shows the advantages of controllable reaction, environmental friendliness and low carbon emissions. The viscosities of the bacterial solution (BS) and cementing solution (CS) in MICP are extremely small, which enables the solution to diffuse larger and deeper than Portland cement and other chemical materials. In addition, the calcium carbonate produced by MICP cannot completely fill the pores, which is beneficial to biological activities and plant growth [33–43]. Moreover, MICP is well adapted to the ocean environment, where the pH is alkaline, and Sporosarcina pasteurii is an alkaliphilic microorganism, Seawater also contains calcium and magnesium ions, which increase the intensity of carbonate precipitation [44,45]. Since Boquet et al. (1973) discovered that some microorganisms in nature can induce the production of calcium carbonate through their own metabolic activities, the reaction mechanism and engineering applications of MICP have been continuously studied over the world [46]. The National Research Council of the United States has even listed MICP technology as a major research topic in the 21st century. Whiffin (2004) first applied MICP technology to reinforce loose sand to improve the strength and stiffness [47]. Michell and Santamarina (2005) further clarified that MICP technology has broad application value and potential in engineering [48].

To date, MICP technology has been widely used in the fields of ground improvement [49–60], erosion control [61–77], crack repair [78–83], liquefaction mitigation [84–93], corrosion protection [94,95], etc. There are a large number of review articles that have comprehensively summarized MICP from the aspects of technical principles, influencing factors, application scenarios, and reinforcement efficiency [96–106], but there has been no comprehensive review of MICP technology in ocean engineering. Therefore, this review focuses on erosion and liquefaction control in the field of ocean engineering, and conducts a comprehensive analysis from the traditional biomineralization process, optimization, erosion control of coastline, local scour protection around monopile, and stability evaluation of MICP-treated seabed. Through an in-depth discussion of key points, comments and suggestions on current research gaps and potential future steps are provided.

2. Biomineralization Process and Efficiency Optimization

2.1. Traditional Biomineralization Process

The traditional biomineralization process, particularly MICP, leverages the metabolic activity of ureolytic bacteria most notably *Sporosarcina pasteurii* to precipitate calcium carbonate ($CaCO_3$) in porous media [107]. This process involves two critical biochemical reactions (Figure 2a):

(1) Ureolysis: Sporosarcina pasteurii hydrolyzes urea into ammonium (NH_4^+) and carbonate ions (CO_3^{2-}) via the enzyme urease:

$$CO(NH_2)_2 + 2H_2O \xrightarrow{bacteria} 2NH_4^+ + CO_3^{2-} \quad (1)$$

 doi:10.20944/preprints202505.1387.v1

(2) Calcium carbonate precipitation: The generated CO32- reacts with free calcium ions (Ca^{2+}) to form calcium carbonate:

$$CO_3^{2-} + Ca^{2+} \rightarrow CaCO_3 \downarrow \quad (2)$$

These reactions occur optimally at pH 7-9, driven by bacterial mineralization capacity and site-specific geochemical conditions. The $CaCO_3$ crystals nucleate heterogeneously on microbial cell walls or sediment particles, progressively cementing soil grains and filling pore spaces (Figure 2b).

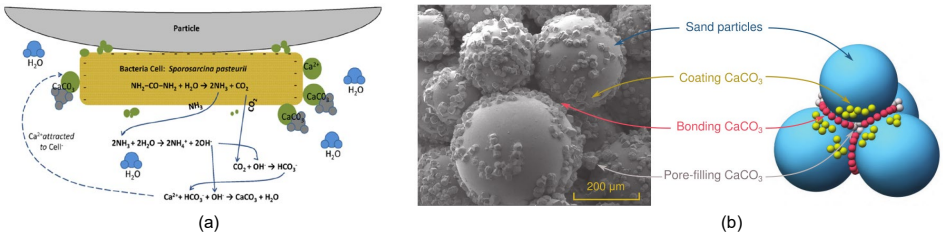

Figure 2. (a) Schematic of MICP process via ureolysis (DeJong et al., 2020), (b) images of CaCO3 precipitation pattern [108].

The efficiency of biomineralization hinges on microbial metabolic activity, substrate availability, and environmental adaptability. Urease activity directly correlates with reaction kinetics. For instance, Sporosarcina pasteurii exhibits urease activity with a Vmax of 3.55 mM urea hydrolyzed min-1·mg-1 at pH 7.0 and 25°C under optimal growth conditions, demonstrating significantly faster microbiological $CaCO_3$ precipitation compared to chemical processes [109]. At present, a large number of calcium carbonate sediments have been found in ocean environment, from coastlines to seabed sediments, they generally come from organic life forms such as corals and show obvious biological characteristics [110,111]. They interact with the complex ocean environment through the mineralization of urease-producing microorganisms in the coastlines and seabed and eventually precipitation. This type of sediment preserves good strength characteristics and porosity, providing an excellent shelter for the survival of organisms on coastlines and seabed. However, it should be noted that under natural conditions, the formation of carbonate precipitation generally takes a long time, which mainly depends on the urease activity of bacteria, reactant concentration, temperature, humidity, oxygen and other conditions. Especially in the ocean environment, how to intensify the process of biomineralization through artificial intervention and form technology that is beneficial to us is a question worth considering.

2.2. Biomineralization Efficiency Optimization

One of the major issues that needs to be solved in the application of MICP technology is the uniformity of cementation. Uneven cementation will lead to stress concentration and brittle failure of the reinforced ground when subjected to load. Many scholars have conducted research and analysis on this issue. Three methodologies were evaluated by Kang et al. (2025) for MICP in silt cementation [112]. The mixing method, involving direct blending of bacterial and cementation solutions with silt prior to compaction, achieved optimal uniformity and strength (801.25 kPa UCS). This approach ensured even radial and longitudinal $CaCO_3$ distribution, effectively minimizing pore volume disparities. In contrast, the grouting method utilized pressure-driven injection, resulting in longitudinal inhomogeneity with declining $CaCO_3$ content (bottom-to-top gradients) and reduced strength (684.78 kPa UCS), attributed to pore channel clogging hindering upward slurry migration. The immersion method, which soaked silt in solutions, exhibited radial inhomogeneity as $CaCO_3$ precipitation decreased from outer to inner layers due to limited permeability, yielding the lowest strength (206.11 kPa UCS). While adjusting grouting pressure, solution concentration, or utilizing intermittent injection cycles could enhance solute distribution, the study identified mixing as the most effective strategy for uniform cementation. Structural analyses confirmed that mixing generated homogeneous pore networks with spatially consistent $CaCO_3$, whereas grouting and immersion

 doi:10.20944/preprints202505.1387.v1

produced strength variations dictated by solute transport limitations and gradient-dependent precipitation patterns. In addition to methodology optimization, material formulation can also be optimized. Zhu et al. (2025) developed a novel one-phase injection method integrated with polycarboxylic acid (PA) to optimize the uniformity and strength of MICP-treated sand [113]. By leveraging PA's dual functionality, delaying $CaCO_3$ nucleation through Ca^{2+} chelation and acting as a non-bacterial nucleation template, this approach allows deeper penetration of solutions into pores before precipitation begins. Experiments demonstrated that 3% PA delayed initial $CaCO_3$ precipitation by over 2 hours (Figure 3a), enabling uniform reactant distribution, while calcium ion conversion rate curves (Figure 3b) confirmed complete Ca^{2+} utilization within 24 hours under optimal conditions (3% PA added), achieving a strength of 2.76 MPa after five treatment cycles. Comparative analyses revealed PA-MICP's superiority over traditional methods like grouting and immersion, which suffered from pore clogging and radial heterogeneity. Figure 3c further illustrates the efficacy of PA by mapping calcium carbonate distribution in sand columns, showing progressively enhanced homogeneity and cementation coverage with increasing PA concentrations (0%, 1%, 3%, 5%) and extended treatment times, ultimately validating PA's role in bridging soil particle gaps for structural reinforcement.

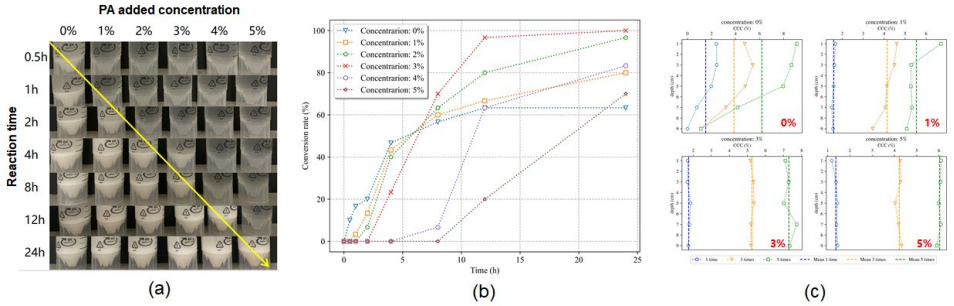

Figure 3. (a) real-time reaction diagram of tube test, (b) conversion rate of calcium ions versus time under different PA addition, and (c) calcium carbonate distribution in sand column under different PA addition and treatment times [113].

3. Multi-Investigations Of Biomineralization Erosion Control in Ocean Engineering

3.1. Erosion Control of Coastline

MICP technology has gradually been applied in the field of erosion control of coastline. Many scholars have systematically evaluated the erosion resistance of MICP-treated sand through unit tests, model tests and field verifications.

According to Clarà Saracho et al. (2020) [114], the erosion resistance of fine sand treated with MICP was systematically evaluated using an erosion function apparatus in Cambridge (EFA in Figure 4a). As shown in Figure 4b-c, untreated sand exhibited rapid surface erosion under tangential flow, with cumulative height loss escalating linearly under incremental shear stress. In contrast, MICP-treated sand (0.02 M urea-calcium solution) demonstrated reduced cumulative erosion by up to 90% due to calcium carbonate crystal cementation. X-ray computed tomography revealed that calcium carbonate filled pore space and formed inter-particle bridges, diminishing erodibility by altering the failure mechanism from particulate detachment to block erosion. Higher cementation concentrations (0.04~0.1 M urea-calcium solution) promoted larger, lognormally distributed crystals (up to 210 μm diameter), which enhanced aggregate stability. This microstructural evolution-linked to microbial metabolism and size-dependent crystal growth-significantly improved macro-scale resistance. The non-monotonic trend declines in erodibility (κ_d) with increased calcium carbonate content underscores MICP's potential in stabilizing vulnerable interfaces in dams or offshore

 doi:10.20944/preprints202505.1387.v1

reservoirs. Future optimizations could target crystal uniformity and injection protocols to maximize erosion control while balancing permeability retention.

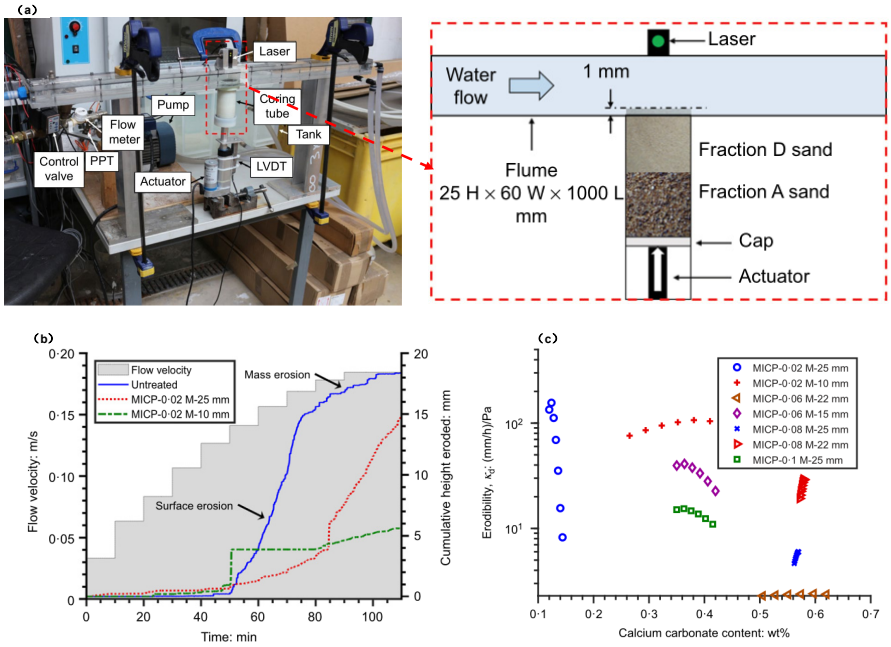

Figure 4. Erosion control of soil (a) EFA experimental set-up, (b) cumulative height eroded-time series for MICP-treated sand, and (c) erodibility plotted against calcium carbonate content [114].

At the model scales, slope erosion tests during tidal actions were conducted by Salifu et al. (2016) [115]. As shown in Figure 5, untreated natural sandy slopes subjected to tidal cycles rapidly collapse to their angle of repose (35°), losing ~0.2° per tidal event. However, MICP-treated slopes (using Sporosarcina pasteurii and 0.7 M $CaCl_2$-urea) resisted collapse by forming a bio-cemented crust (118~155 kg $CaCO_3/m^3$). At 35° inclinations, treatment reduced erosion significantly, while steeper 53° slopes showed negligible erosion despite high shear stresses. The mechanism stems from urea hydrolysis-driven calcite precipitation, forming a bio-cemented crust that withstood tidal shear stresses. SEM and penetration tests confirmed that calcite bridges increased interparticle friction and cohesion. Afterwards, slope erosion tests during wave actions were also conducted by Kou et al. (2020) [116], results were shown in Figure 6. Wave actions on untreated sandy slopes induced rapid particle detachment, forming bilinear erosion profiles. MICP treatment (4 cycles of 0.5 mL/cm2 bacterial and cementation solutions) reduced erosion rates by up to 97%, with calcium carbonate content correlating inversely with mass loss. Penetration resistance (up to 60 kN/m^2) and SEM analyses revealed calcium carbonate's dual role: nano-crystals filled pores, while macroscale aggregates (100-240 μm) formed load-bearing networks. Notably, higher treatment cycles (e.g., 4 cycles) yielded 30.1% $CaCO_3$ content, reducing erosion rates to <1 mm/h under wave velocities of 0.4 m/s. The nonlinear relationship between treatment cycles and erosion resistance highlights a threshold (beyond ~0.08 M Ca^{2+}) where excessive crystal size may paradoxically weaken cohesion. The erosion rate of bio-cemented sandy slope R_e, which represents the erosion resistance, also shows linearly increasing trend with the increase of the treatment cycle N because of $CaCO_3$ formed. In order to more accurately simulate wave breaking on the coastline and analyze the erosion resistance of MICP-reinforced slopes, a series of large-section flume tests were carried out by Li et al. (2020a) [117]. The experiments evaluated erosion patterns, penetration resistance, $CaCO_3$ distribution, and pore water pressure under varying MICP treatment cycles (0, 2, 4) and wave heights (8, 10, 12 cm). Results show that four MICP treatments formed a robust cementation layer on sandy slope, eliminating visible erosion after 60 minutes of wave action (Figure 7). The maximum erosion depths on the slope under the untreated slope, the 2-times MICP-treated slope, and the 4-times MICP-treated slope are 6 cm, 5 cm, and 0, respectively. Penetration resistance increased dramatically from 0.14 MPa

 doi:10.20944/preprints202505.1387.v1

(untreated) to 2.04 MPa (4-times treated), linked to surface CaCO3 content reaching 7% via acid washing tests. The calcium carbonate content of the MICP-treated area decreases from the toe to the top of the slope because of that bacterial and cementation solutions flow from the top to the toe due to gravity. With the increase in MICP treatment times, the permeability of the slope is gradually decreased, resulting in difficult infiltration of bacterial solution, cementation solution, and oxygen. Therefore, the difference in bacterial solution, cementation solution, and oxygen content between the deep and the shallow layer of the slope is increased, leading to the increased difference of calcium carbonate content. MICP treatments form $CaCO_3$ crystals between sand particles, reducing permeability and restricting water pressure transfer. Consequently, Figure 15c shows thickened excess pore water pressure gradients in surface layers of treated slopes compared to untreated ones, highlighting limited fluid mobility.

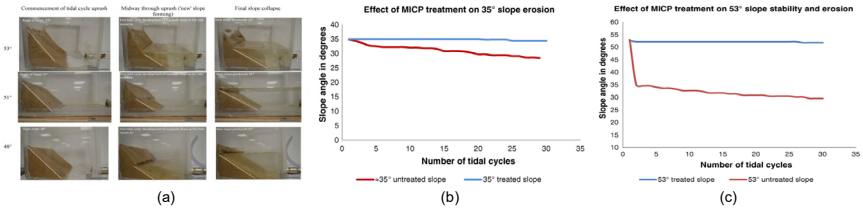

Figure 5. (a) slope erosion during tidal actions, (b) comparing effect of MICP treatment on 35° slope erosion, and (c) comparing effect of MICP treatment on 53° slope erosion.

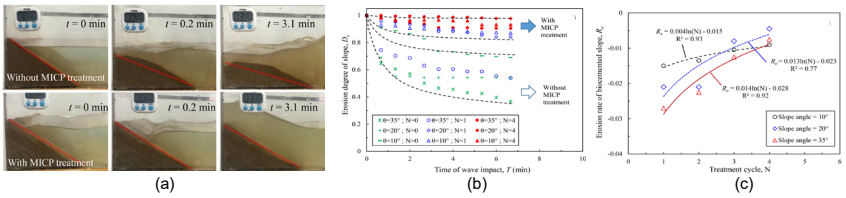

Figure 6. (a) slope erosion during wave actions, (b) erosion degree as a function of time, and (c) effect of treatment cycle on erosion rate of bio-cemented slope [116].

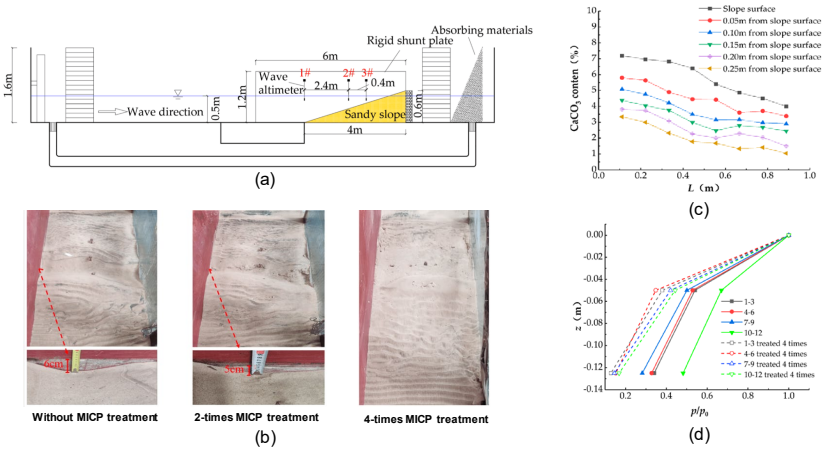

Figure 7. Large-scale flume test (a) experimental design, (b) erosion degree under 10 cm wave height actions, and (c) $CaCO_3$ distribution of MICP-treated sandy slope, and (d) normalized pore water pressure distribution along slope depth under 12 cm wave height [117].

Some field implementations were also conducted to evaluate the erosion resistance of coastline slope treated by MICP. As shown in Figure 8, the Ahoskie study focused on a sandy slope with poor grading, employing three MICP delivery methods: surface spraying, prefabricated vertical drains (PVDs), and shallow gravel-packed trenches [118]. Surface spraying applied urea-$CaCl_2$ solutions

 doi:10.20944/preprints202505.1387.v1

twice daily via an irrigation system with 25 nozzles, forming a uniform surface crust through sequential bacterial solution and cementation solution cycles over 14 days. PVDs (30 cm depth) facilitated vertical seepage, leveraging gravity to transport solutions deeper into the soil, while trenches (60 cm long, 15 cm deep) with pea gravel backfill created localized high-strength zones. Dynamic cone penetration (DCP) tests post-treatment revealed a 73% reduction in surface penetration resistance (0-10 cm) for sprayed areas, with a 2.5-14.5 cm crust containing 7% $CaCO_3$. PVDs enhanced deeper layers, achieving 48% surface and 72% subsurface (30 cm) improvements, while trenches exhibited concentrated strength gains near gravel interfaces, reaching 9.9% $CaCO_3$ content. Remarkably, the treated slope resisted erosion during Hurricane Dorian, maintaining integrity over 331 days due to the crust's durability and permeability retention, which supported natural vegetation recovery. As shown in Figure 9, the Sanya implementation expanded this research to tidal environments, comparing MICP and EICP performance under seawater and freshwater conditions. At Yazhou Bay, a coastal sandy slope was divided into atmospheric and tidal zones, treated using dual-nozzle sprayers for MICP (*Sporosarcina pasteurii* cultures) or EICP (urease enzymes) developed by authors with 1M concentration urea-$CaCl_2$ solutions. Seawater-based solutions (34.9‰ salinity) were tested against freshwater variants to explore marine adaptability. In the atmospheric zone, MICP-treated zone by seawater achieved 1743 kPa penetration resistance (vs. 35-85 kPa untreated zone) with a 17 cm crust (9.9% $CaCO_3$), reducing erosion by 0.197 m^3 compared to untreated zone (0.393 m^3 loss). EICP-treated zone by freshwater yielded lower but significant resistance, about 560 kPa (8.1% $CaCO_3$). In tidal zones, wave and saltwater exposure degraded protection performance, seawater-MICP peaked at 493 kPa but reverted to baseline within 24 days. However, tidal flow induced layered $CaCO_3$ deposition ("M-shaped" profile at 5-15 cm depth) and net sediment deposition (0.054-0.197 m^3 retention vs. untreated 0.29 m^3 erosion). Microstructural analysis via SEM highlighted spherical $CaCO_3$ crystals (5-20 μm) in MICP-treated zone, bridging sand grains, while EICP produced smaller, irregular aggregates.

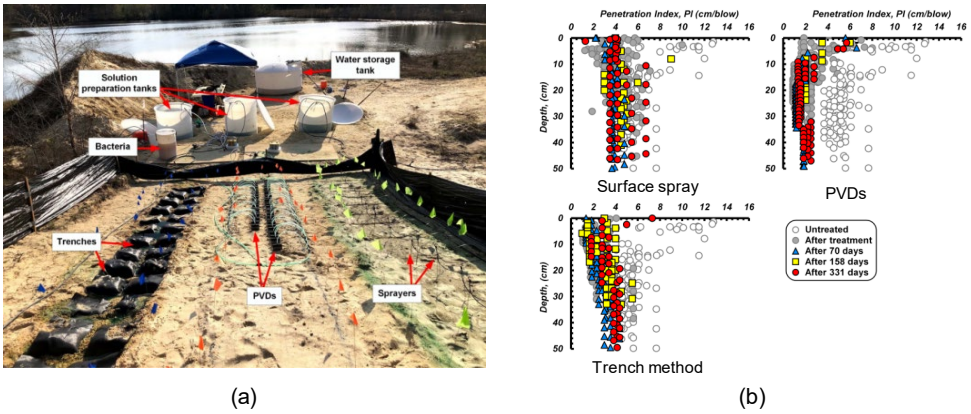

Figure 8. Field implementation of MICP for erosion reduction of coastline sandy slope in Ahoskie, North Carolina (a) overall view of field design, (b) DCP results of slope under different treatment, surface spraying, PVDs and trench method [118].

 doi:10.20944/preprints202505.1387.v1

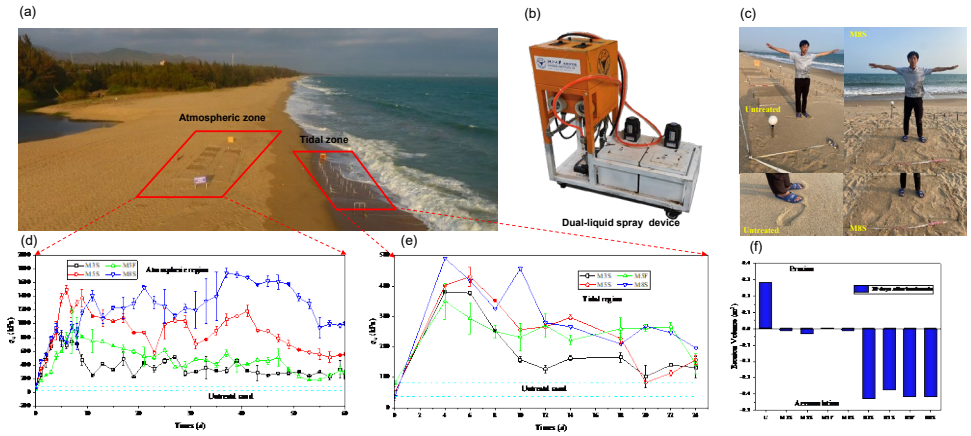

Figure 9. Field implementation of MICP and EICP for erosion reduction of coastline sandy slope in SanYa, Hainan (a) overall view of field design, (b) double liquid spray equipment, (c) visual observation of reinforcement effect, (d) evolution of the penetration resistance in atmospheric region, (e) evolution of the penetration resistance in tidal region, and (f) erosion volume in tidal region at 20 days after treatments [119].

These studies collectively demonstrate MICP's transformative potential in coastline erosion control through biomineralization, offering an eco-friendly alternative to conventional coastal protection methods when environmental requirements have to be considered.

3.2. Local Scour Protection Around Monopile

This section summarized the local scour protection around monopile treated by MICP. Li et al. (2022b) investigated the efficacy of MICP for mitigating local scour around monopile foundations under unidirectional currents [120]. The experiments were conducted in a large-scale flume using silica sand (d_{50}= 0.16 mm) treated with MICP technology. MICP treatments involved sequential spraying of bacterial solution (OD600 = 2.0, urease activity = 20 U/mL) and cementation media (1M urea/1M $CaCl_2$) 1-4 times over 4 days. For comparison, traditional riprap protection (5-10 mm gravel) was also tested. A non-contact camera system and handheld 3D scanners monitored scour evolution and post-test topography. Sediment transport rates were calculated using acid-washed CaCO3 content and SEM analysis. As shown in Figure 10, 2-times MICP treatments reduced maximum scour depth (S_{end}/D_P) by 84% (from 1.14D_P in untreated sand to 0.18D_P), 4-times treatments eliminated visible scour holes under 0.3 m/s live-bed conditions, while riprap protection achieved only 0.38D_P. The D_P represents the diameter of the monopile. Penetration resistance increased exponentially with treatment cycles N. Surface $CaCO_3$ content reached 3.8%, forming an inverted cone-shaped cemented layer (height = 4-9 cm) that resisted downflow and horseshoe vortices. Sediment transport rate dropped by 53% (from 19.4 kg/m/h to 9 kg/m/h at pile proximity), attributed to $CaCO_3$ bridging effects (spherical crystals, 5-20 μm). However, the maximum edge scour depth (length) increases from 0.19 (3.18) D_P to 0.29 (4.36) D_P after 2-times to 4-times MICP treatments. It is necessary to consider the balance of MICP protective times and edge scour. Zhu et al. (2024) investigated the lateral response of offshore monopiles reinforced by MICP through static and cyclic loading tests [121]. Key findings reveal that precast bio-reinforcement (4D_P width and 1D_P depth) enhances the lateral bearing capacity by 50% and reduces maximum bending moments by 25%, transitioning failure modes from localized to global overturning. Under cyclic loading, accumulated deformation decreased by 30-60% for one-way loading, with secant stiffness ratios (MICP-treated vs. untreated) ranging 1.65-2.82 (higher under smaller loads). Mechanistically, MICP-treated sand improved shallow soil resistance, but stiffness evolution was governed by three competing factors: untreated sand compaction, bio-cementation degradation at low strains, and soil subsidence around the reinforced zone. The low-pH grouting method demonstrated eco-friendly advantages over

 doi:10.20944/preprints202505.1387.v1

traditional cementation, offering a sustainable solution to optimize monopile dimensions for offshore wind turbines while balancing cyclic durability and environmental impact.

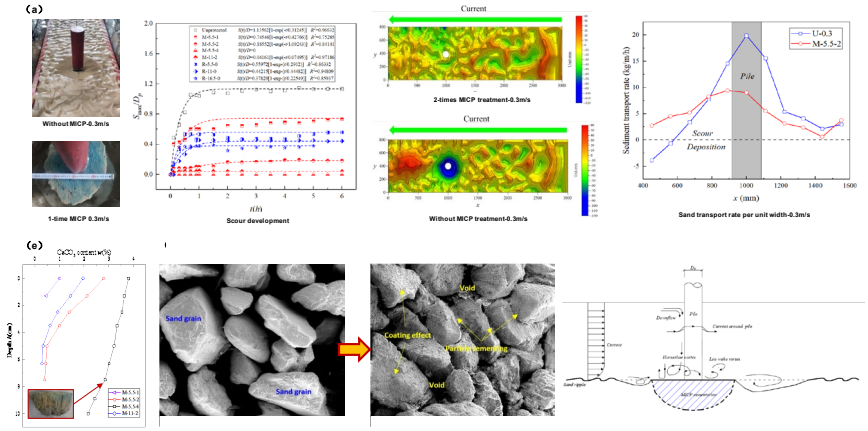

Figure 10. Local scour of MICP protection around monopile (a) visual observation, (b) scour depth evolution under different protection method, (c) terrain scanning after scour, (d) sediment transport rate at different location, (e) $CaCO_3$ distribution along depth, (f) SEM of sand without MICP treatment, (g) SEM of sand after MICP treatment, (f) Erosion resistance mechanism of MICP protection [120].

Separately, Wang et al. (2020) evaluated the erosion protection effectiveness of polyvinyl alcohol (PVA) coupling MICP technology for bridge pier local scour through scale model flume experiments (Figure 10) [122]. A 3D-printed pier model (12×3×16 cm) was embedded in PVA-MICP-treated Ottawa sand stratum and subjected to 20-hour continuous flow simulation at 0.15 m/s (70% of untreated sand's critical velocity). Results demonstrated that untreated sand developed a 25 mm horseshoe-shaped scour hole stabilizing within 2 hours, while PVA coupling MICP-treated sseabed maintained minimal erosion (<0.3 mm) with structural integrity. Microscopic characterization (SEM/XRD) revealed that PVA viscosity modulation facilitated dense distribution of 2-3 μm vaterite-type $CaCO_3$ crystals at particle contacts, significantly enhancing interlayer cementation strength. Erosion Function Apparatus (EFA) quantification showed modified sand exhibited 500-fold increased critical shear stress (94.4 Pa vs. 0.18 Pa for untreated sand), sustaining low erosion rate (0.1 mm/h) under extreme 6 m/s flow velocity. Structure from Motion (SEM) topographic reconstruction confirmed over 95% reduction in sediment loss from treated zones, demonstrating that PVA's delayed infiltration effectively controlled cementation layer thickness (~5 cm) through single surface application without deep grouting.

 doi:10.20944/preprints202505.1387.v1

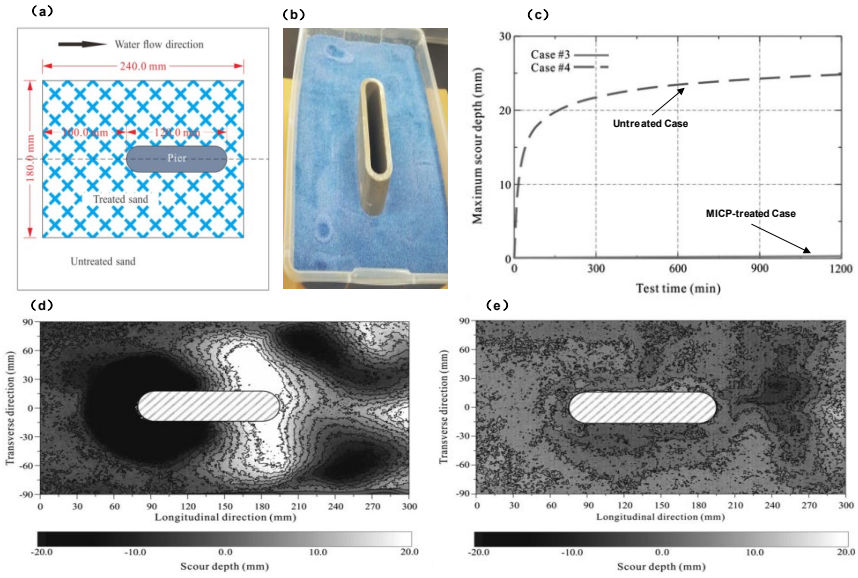

Figure 11. Polyvinyl alcohol (PVA) coupling MICP for local scour protection around monopile (a) test design, (b) actual image, (c) comparison of protection effect, (d) terrain scanning of case without protection after scour, and (e) terrain scanning of case with protection after scour [122].

MICP and PVA coupling MICP effectively mitigate local scour around monopile through biomineralization and polymer-enhanced crystal adhesion. Their success hinges on controlled reagent, optimized treatment cycles, and geometric design to balance erosion resistance and edge scour.

3.3. Stability Evaluation of MICP Reinforced Seabed

In addition to erosion protection, MICP technology can also be used to reinforce the seabed and improve stability. Considering the high cost and control difficulty of the physical experiments, numerical simulation was first developed for analysis. To date, numerical studies on MICP reaction are mainly based on the convection-diffusion-reaction theory and seepage framework in porous media. Martinez et al. (2014) used the first-order kinetic equation to establish a reaction model of urea hydrolysis and calcium carbonate precipitation, but ignored the effect of calcium carbonate precipitation on the evolutions of porosity and permeability [123]. Fauriel and Laloui (2012), Wang and Nackenhorst (2020) established a bio-chemo-hydro-mechanical model for MICP reaction and a bio-chemo-hydro model considering the concept of effective porosity, respectively [124,125]. Recently, a bio-chemo-hydro-mechanical model of transport, strength and deformation for bio-cementation applications was developed by Bosch et al. (2024) to design MICP treatments for specific geotechnical problems, such as bearing capacity [126]. Although the above models well reflect the temporal and spatial evolutions of biochemical substances and permeability in the MICP reaction, it is not applicable to the ocean environment because of the neglect of the ocean dynamic environment factors.

Li developed a MICP reaction model for seabed reinforcement considering the wave actions under the framework of Biot's consolidation equation [128,129]. According to the existence form of bacteria in seabed, the total bacteria (C_{total}) are divided into suspended bacteria (C_{bacl}) attached bacteria (C_{bacs}) on the sand particle surface, assuming that they satisfy the first-order kinetic equation:

$$\frac{\partial C_{bact}}{\partial t} = -k_d C_{bact} \quad (3)$$

$$\frac{\partial C_{bacs}}{\partial t} = k_{att} C_{bacl} - k_d C_{bacs} \quad (4)$$

$$\frac{\partial C_{bacl}}{\partial t} = -k_{att} C_{bacl} - k_d C_{bacl} \quad (5)$$

 doi:10.20944/preprints202505.1387.v1

where k_d is a constant decay rate, and k_{att} is the constant attachment rate. Urea hydrolysis is described with the adoption of the Michaelis-Menten kinetic equation.

$$k_{\mathrm{rea}} = u_{\mathrm{sp}}(C_{bacs} + C_{bacl}) \cdot \frac{C_{\mathrm{urea}}}{C_{\mathrm{urea}}+k_{\mathrm{m}}} \cdot \exp\left((T-25)/\frac{\ln 3.4}{10}\right)\exp\left(-\frac{t}{t_{\mathrm{d}}}\right) \quad (6)$$

where k_m, T, u_{sp}, C_{urea}, t, t_d represents the half-saturation constant when the reaction rate is reduced by 50%, the environment temperature, the maximum urease constant, the concentration of urea, reaction time and time constant.

The Darcy's law is used to describe the hydraulic field.

$$\boldsymbol{q} = -\frac{K}{\mu_{\mathrm{l}}} \cdot (\nabla p_{\mathrm{l}} + \rho_{\mathrm{l}}\boldsymbol{g}) \quad (7)$$

where $\boldsymbol{q}$ is the Darcy flow rate, K is the matrix permeability, $\boldsymbol{g}$ is the gravity acceleration, and the μ_l, p_l, and ρ_l represent the liquid viscosity, excess pore pressure as well as the liquid density, respectively. All the liquid substances (urea, calcium, ammonium and suspend bacteria) are assumed to be controlled by convection-diffusion-reaction equations, as shown in equations 8-11.

$$\varphi\frac{\partial C_{\mathrm{urea}}}{\partial t} = \nabla \cdot (\varphi \boldsymbol{D}^* \cdot \nabla C_{\mathrm{urea}}) - \boldsymbol{q} \cdot \nabla C_{\mathrm{urea}} - \varphi k_{\mathrm{rea}} \quad (8)$$

$$\varphi\frac{\partial C_{\mathrm{NH_4^+}}}{\partial t} = \nabla \cdot \left(\varphi \boldsymbol{D}^* \cdot \nabla C_{\mathrm{NH_4^+}}\right) - \boldsymbol{q} \cdot C_{\mathrm{NH_4^+}} + 2\varphi k_{\mathrm{rea}} \quad (9)$$

$$\varphi\frac{\partial C_{\mathrm{Ca^{2+}}}}{\partial t} = \nabla \cdot (\varphi \boldsymbol{D}^* \cdot \nabla C_{\mathrm{Ca^{2+}}}) - \boldsymbol{q} \cdot C_{\mathrm{Ca^{2+}}} - \varphi k_{\mathrm{rea}} \quad (10)$$

$$\varphi\frac{\partial C_{\mathrm{bacl}}}{\partial t} = \nabla \cdot (\varphi \boldsymbol{D}^* \cdot \nabla C_{\mathrm{bacl}}) - \boldsymbol{q} \cdot C_{\mathrm{bacl}} - \varphi k_{\mathrm{d}} C_{\mathrm{bacl}} - \varphi k_{\mathrm{att}} C_{\mathrm{bacl}} \quad (11)$$

where C_i represents the concentration of the liquid component, i includes the urea, calcium, ammonium and suspended bacteria, $\boldsymbol{q}$ and $\boldsymbol{D}^*$ (tensor) represent the Darcy velocity and hydrodynamic dispersion coefficient in seabed. The value of $\boldsymbol{D}^*$ depends on pore velocity, dispersivity, pore tortuosity, pore size and solute concentration gradient. The Fick's law is adopted to consider the diffusion of chemical substances overflowing from the seabed surface into seawater, as shown in equations 12-15.

$$\frac{\partial C_{\mathrm{urea}}}{\partial t} = \nabla \cdot (\boldsymbol{D} \cdot \nabla C_{\mathrm{urea}}) \quad (12)$$

$$\frac{\partial C_{\mathrm{NH_4^+}}}{\partial t} = \nabla \cdot \left(\boldsymbol{D} \cdot \nabla C_{\mathrm{NH_4^+}}\right) \quad (13)$$

$$\frac{\partial C_{\mathrm{Ca^{2+}}}}{\partial t} = \nabla \cdot (\boldsymbol{D} \cdot \nabla C_{\mathrm{Ca^{2+}}}) \quad (14)$$

$$\frac{\partial C_{\mathrm{bacl}}}{\partial t} = \nabla \cdot (\boldsymbol{D} \cdot \nabla C_{\mathrm{bacl}}) \quad (15)$$

where $\boldsymbol{D}$ (tensor) represents the hydrodynamic dispersion coefficient in water phase, the value of $\boldsymbol{D}$ is always taken as 2×10-9 m²/s. The decrease of the total porosity and the increase of the calcium carbonate can be described by

$$\frac{\partial \varphi_{\mathrm{tot}}}{\partial t} = -\frac{1}{\rho_{\mathrm{c}}} m_{\mathrm{CaCO_3}} \varphi_{\mathrm{tot}} k_{\mathrm{rea}} \quad (16)$$

$$\frac{\partial C_{\mathrm{CaCO_3}}}{\partial t} = m_{\mathrm{CaCO_3}} \varphi_{\mathrm{tot}} k_{\mathrm{rea}} \quad (17)$$

The Kozeny-Carman (KC) equation is adopted to describe the relationship between porosity and permeability. The concept of the effective porosity and the modified KC equation were adopted in this model [125,127].

$$x = \frac{\varphi_{\mathrm{tot}}-\varphi_{\mathrm{c}}}{1-\varphi_{\mathrm{c}}} \quad (18)$$

$$\varphi_{\mathrm{eff}} = ax^3 - (2a+\varphi_{\mathrm{c}})x^2 + (a+1+\varphi_{\mathrm{c}})x \quad (19)$$

$$k_{\mathrm{i}} = k_0 \frac{((\varphi_{\mathrm{eff}})_{\mathrm{i}})^3}{(1-(\varphi_{\mathrm{eff}})_{\mathrm{i}})^2} \frac{(1-(\varphi_{\mathrm{eff}})_0)^2}{((\varphi_{\mathrm{eff}})_0)^3} \quad (20)$$

where i represents the current time step, k_i and k_0 are the current permeability and initial permeability, $(\varphi_{eff})_i$ and $(\varphi_{eff})_0$ represent the current effective porosity and initial effective porosity.

For homogeneous and isotropic seabed, the theoretical equations are as follows [130]

$$G\frac{2-2\nu}{1-2\nu}\frac{\partial^2 u}{\partial z^2} = \frac{\partial p}{\partial z} \quad (21)$$

$$\frac{k}{\gamma_{\mathrm{w}}}\frac{\partial^2 p}{\partial z^2} = \frac{\partial^2 u}{\partial z \partial t} + \varphi\beta\frac{\partial p}{\partial t} \quad (22)$$

where G is the shear modulus of the seabed, which increases with the increase of the calcium carbonate content. z is the vertical coordinate axis, the origin of which is on the seabed surface with the positive direction downwards. u is the soil displacement, υ is the Poisson's ratio, p is the excess

 doi:10.20944/preprints202505.1387.v1

pore pressure. k, γ_w, φ, and β represent the permeability coefficient, water weight, seabed porosity, and the effective compressibility of the combined liquid-gas.

$$\beta = \left(\frac{1}{K_f} + \frac{1-S_r}{p_{w0}}\right) \quad (23)$$

where S_r is the saturation degree of the seabed, p_{w0} is the absolute static pressure and K_f is the bulk modulus of the pore water. The pore pressure p affects the Darcy velocity, thus affecting the convection-diffusion-reaction process and the precipitation of calcium carbonate. Conversely, the $CaCO_3$ precipitation clogs the pores, reduces permeability, and increases the shear modulus, which in turn affects the Biot's dynamic response. Therefore, this MICP numerical model considering wave actions is a bidirectional coupled nonlinear system.

Li et al. (2023) first verified the correctness of this numerical model through unit tests, and then carried out a large number of calculations [128]. The results showed that the MICP process increased the excess pore pressure gradient and vertical effective stress amplitude of seabed (Figure 12b). This is mainly due to the blockage of the seabed surface soil by the precipitation of calcium carbonate, which makes it bear greater seepage force. As shown in Figure 12c, the maximum instability depth of the untreated seabed increases with the increase of the wave height. If cohesive force F_c is ignored, the MICP treated seabed started to be unstable when the wave height reached 2 m. When inner cohesive force Fc is considered, the seabed remained stable under 4 m wave height. These results indicate that MICP plays a vital role in keeping the seabed stable under the wave actions.

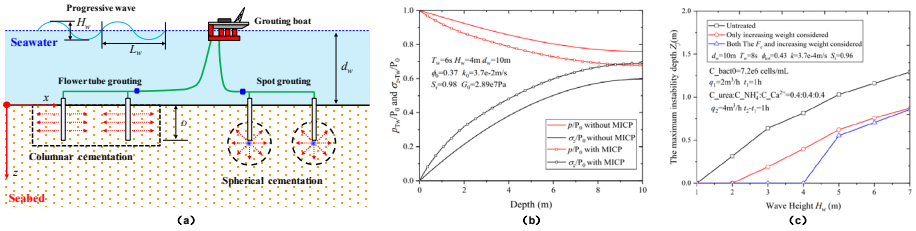

Figure 12. Liquefaction mitigation of seabed (a) Schematic diagram, (b) the influence of MICP on the dynamic response of seabed, and (c) the influence of wave height on the maximum instability depth [128].

4. Suggestions for Future Research

Although MICP technology has been applied to control erosion and liquefaction in ocean engineering, from units, models to a small number of fields, there are still issues should be considered such as low reinforcement efficiency, insufficient reinforcement durability, and possible foreign microbial invasion concerns. In addition, current experimental researches have basically ignored the mutual coupling effects of MICP reaction and common ocean dynamic environmental elements such as wave and current. Therefore, subsequent research can be carried out from the following aspects: 1) Indigenous bacteria capable of producing urease can be screened out from the ocean environment. Subsequently, gene editing techniques will be employed to achieve overexpression of the urease gene, analyze the mineralization rate and effects on indigenous bacterial communities of this bacteria, then obtain indigenous bacteria with high urease production; 2) investigate the interaction between common ocean dynamic environmental elements and the MICP reaction through multi-scale research, then analyze the erosion of liquefaction resistance of MICP-treated soil. 3) investigate the real effect of MICP in coastline erosion protection and liquefaction mitigation through long-term field tests.

5. Conclusions

This paper comprehensively reviews recent advancements in MICP for erosion control and liquefaction mitigation in ocean engineering, synthesizing multi-scale experiments, field applications, and coupled numerical modelling. The efficacy of biomineralization in diverse scenarios, including coastal slope stabilization, local scour mitigation, and seabed reinforcement

 doi:10.20944/preprints202505.1387.v1

under wave actions are evaluated systematically, the suggestions for future researches are also proposed. The specific conclusions are as follow:

(1) The optimization of reinforcement methodology (mixing, grouting, immersion) and material formulation (polycarboxylic acid, PA) are conducive to a more uniform distribution of calcium carbonate. The addition of 3% polycarboxylic acid (PA) delays the onset of $CaCO_3$ precipitation by >2 hours and acts as a non-bacterial nucleation template, facilitating spatially uniform distribution. Kinetic analysis of Ca^{2+} conversion confirmed complete ion utilization within 24 hours under optimized PA concentration (3%), yielding a compressive strength of 2.76 MPa after five treatment cycles.

(2) The erosion resistance of coastline soil was investigated by erosion function apparatus (EFA) tests, tidal actions model test, wave actions model test and field applications. Field validations in Ahoskie and Sanya demonstrate the efficacy of MICP in coastal erosion control through tailored delivery systems and environmental adaptations. In Ahoskie, three delivery methods (surface spraying, PVDs, and trenches) achieved distinct performance: surface spraying formed a 7% $CaCO_3$ crusts (73% surface strength improvement), PVDs enhanced subsurface layers (72% improvement at 30 cm depth), and trenches concentrated CaCO3 (9.9%) near gravel interfaces, collectively enabling the slope to withstand Hurricane Dorian over 331 days. Meanwhile, Sanya's studies highlighted seawater-compatible MICP solutions, achieving maximum 1743 kPa penetration resistance in atmospheric zone and layered "M-shaped" $CaCO_3$ precipitation in tidal regions. Comparatively, EICP under freshwater yielded weaker aggregates, with MICP's spherical crystals outperforming EICP's irregular structures. While tidal exposure degraded MICP durability, synergies between biomineralization and natural sedimentation underscored its ecological potential.

(3) MICP coupled with polyvinyl alcohol (PVA) effectively mitigate local scour around monopile through biomineralization and polymer-enhanced crystal adhesion. Experimental studies reveal that MICP treatments (2-4 cycles) reduce maximum scour depth by 84-100% under unidirectional currents through the formation of a 4-9 cm MICP cemented cone stabilizing seabed sediment. It is necessary to consider the balance of MICP protective times and edge scour. MICP coupled with polyvinyl alcohol (PVA) outperforms conventional methods, achieving 500-fold increases in critical shear stress (94.4 Pa) via dense vaterite crystallization at particle contacts and sustaining <0.3 mm erosion under extreme flows. Synergistic effects of polymer-modulated infiltration and biomineralization enable precise 5 cm-thick cemented layers without deep grouting.

(4) In addition to erosion protection, MICP technology can also be used to reinforce the seabed and improve stability. The numerical model of MICP reaction for seabed reinforcement considering the wave actions, incorporating bacterial kinetics (suspended/attached phases), urea hydrolysis (Michaelis-Menten equation), and Darcy-driven convection-diffusion-reaction processes, can be used to analysis the seabed stability after MICP treatment. This framework accounts for $CaCO_3$ induced porosity reduction and shear modulus enhancement, resolving wave-seabed-MICP interactions. Simulations reveal MICP increases seabed stability by amplifying vertical effective stress and reducing pore pressure. Surface $CaCO_3$ clogging diminishes permeability and redistributes seepage forces, enhancing resistance to liquefaction. Comparative analyses confirm untreated seabed instability increases linearly with wave height, while MICP-treated seabed exhibit nonlinear stability gains through cohesive strength effects. Validated via unit tests and parametric studies, the model demonstrates MICP's efficacy in mitigating wave-induced seabed liquefaction.

While MICP shows promise in mitigating erosion and liquefaction in coastline and seabed, challenges persist in treatment efficiency, durability, and ecological risks from non-native microbial contamination. Future research should address: (1) Cultivating indigenous ocean urease-producing bacteria via gene editing to enhance urease overexpression and assess ecological impacts; (2) Multiscale investigations on hydrodynamic-MICP coupling, including flow-driven mass transfer and

 doi:10.20944/preprints202505.1387.v1

long-term biomineralization stability under hydrodynamic actions; (3) Field validations quantifying coastal protection efficacy and biomineralization degradation in tidal/wave zones. Addressing these gaps will optimize eco-compatible MICP protocols for sustainable ocean engineering applications, balancing engineering performance with ecological integrity.

Author Contributions: Data curation, Writing-Original draft preparation, Investigation, Funding acquisition, Shan Liu; Data curation, Writing- Reviewing and Editing, Changrui Dong; Test, Validation, Yongqiang Zhu; Investigation, Methodology, Zichun Wang; Writing- Reviewing and Editing, Investigation, editing, Funding acquisition, Yujie Li; Investigation,Funding acquisition, Guohui Feng

Funding: The authors would like to acknowledge the supports from Science and Technology Project of Water Resources Department of Zhejiang Province (RC2230), National Natural Science Foundation of China (52401344; 52408448), Postdoctoral Fellowship Program of CPSF under Grant Number (GZC20241516).

Institutional Review Board Statement: Not applicable.

Informed Consent Statement: Not applicable.

Data Availability Statement: Not applicable.

Conflicts of Interest: The authors declare that they have no competing financial or non-financial interests that are relevant to the present work.

References

1. Bird, E. C. (1985). Coastline changes. A global review.
2. Zhang, K., Douglas, B. C., & Leatherman, S. P. (2004). Global warming and coastal erosion. Climatic change, 64, 41-58.
3. Zhu, X., Linham, M. M., & Nicholls, R. J. (2010). Technologies for climate change adaptation-Coastal erosion and flooding. Danmarks Tekniske Universitet, Risø Nationallaboratoriet for Bæredygtig Energi.
4. Pilkey, O. H., & Cooper, J. A. G. (2020). The last beach. Duke University Press.
5. Barragán, J. M., & De Andrés, M. (2015). Analysis and trends of the world's coastal cities and agglomerations. Ocean & Coastal Management, 114, 11-20.
6. Ataie-Ashtiani, B., & Beheshti, A. A. (2006). Experimental investigation of clear-water local scour at pile groups. Journal of Hydraulic Engineering, 132(10), 1100-1104.
7. Amini, A., Melville, B. W., Ali, T. M., & Ghazali, A. H. (2012). Clear-water local scour around pile groups in shallow-water flow. Journal of Hydraulic Engineering, 138(2), 177-185.
8. Qi, W. G., Gao, F. P., Randolph, M. F., & Lehane, B. M. (2016). Scour effects on p–y curves for shallowly embedded piles in sand. Géotechnique, 66(8), 648-660.
9. Sumer, B. M., Fredsøe, J., & Christiansen, N. (1992). Scour around vertical pile in waves. Journal of waterway, port, coastal, and ocean engineering, 118(1), 15-31.
10. Qi, W. G., Li, Y. X., Xu, K., & Gao, F. P. (2019). Physical modelling of local scour at twin piles under combined waves and current. Coastal Engineering, 143, 63-75.
11. Sumer, B. M., Whitehouse, R. J., & Tørum, A. (2001). Scour around coastal structures: a summary of recent research. Coastal engineering, 44(2), 153-190.
12. Raudkivi, A. J., & Ettema, R. (1983). Clear-water scour at cylindrical piers. Journal of hydraulic engineering, 109(3), 338-350.
13. Whitehouse, R. (1998). Scour at marine structures: A manual for practical applications. Thomas Telford.
14. Lin, Y., & Lin, C. (2019). Effects of scour-hole dimensions on lateral behavior of piles in sands. Computers and Geotechnics, 111, 30-41.
15. Wang, H., Wang, L., Hong, Y., Mašín, D., Li, W., He, B., & Pan, H. (2021). Centrifuge testing on monotonic and cyclic lateral behavior of large-diameter slender piles in sand. Ocean Engineering, 226, 108299.
16. Guo, X., Liu, J., Yi, P., Feng, X., & Han, C. (2022). Effects of local scour on failure envelopes of offshore monopiles and caissons. Applied Ocean Research, 118, 103007.

 doi:10.20944/preprints202505.1387.v1

17. Yamamoto, T., Koning, H. L., Sellmeijer, H., & Van Hijum, E. P. (1978). On the response of a poro-elastic bed to water waves. Journal of Fluid mechanics, 87(1), 193-206.
18. Sakai, T., Hatanaka, K., & Mase, H. (1992). Wave-induced effective stress in seabed and its momentary liquefaction. Journal of waterway, port, coastal, and ocean engineering, 118(2), 202-206.
19. Mory, M., Michallet, H., Bonjean, D., Piedra-Cueva, I., Barnoud, J. M., Foray, P., ... & Breul, P. (2007). A field study of momentary liquefaction caused by waves around a coastal structure. Journal of Waterway, Port, Coastal, and Ocean Engineering, 133(1), 28-38.
20. Chávez, V., Mendoza, E., Silva, R., Silva, A., & Losada, M. A. (2017). An experimental method to verify the failure of coastal structures by wave induced liquefaction of clayey soils. Coastal Engineering, 123, 1-10.
21. Young, Y. L., White, J. A., Xiao, H., & Borja, R. I. (2009). Liquefaction potential of coastal slopes induced by solitary waves. Acta Geotechnica, 4, 17-34.
22. Wang, Y., Wang, Q., Cao, R., Gao, G., Feng, X., Yin, B., ... & Lv, X. (2025). Pressure characteristics of two-dimensional topography in wave-induced seabed liquefaction. Physics of Fluids, 37(1).
23. Zhao, H. Y., Jeng, D. S., & Liao, C. C. (2016). Parametric study of the wave-induced residual liquefaction around an embedded pipeline. Applied Ocean Research, 55, 163-180.
24. Chen, W., Fang, D., Chen, G., Jeng, D., Zhu, J., & Zhao, H. (2018). A simplified quasi-static analysis of wave-induced residual liquefaction of seabed around an immersed tunnel. Ocean Engineering, 148, 574-587.
25. Kirca, V. O., Sumer, B. M., & Fredsøe, J. (2012, June). Residual liquefaction under standing waves. In ISOPE International Ocean and Polar Engineering Conference (pp. ISOPE-I). ISOPE.
26. Jeng, D. S., Chen, L., Liao, C., & Tong, D. (2019). A numerical approach to determine wave (current)-induced residual responses in a layered seabed. Journal of Coastal Research, 35(6), 1271-1284.
27. Vousdoukas, M. I., Ranasinghe, R., Mentaschi, L., Plomaritis, T. A., Athanasiou, P., Luijendijk, A., & Feyen, L. (2020). Sandy coastlines under threat of erosion. Nature climate change, 10(3), 260-263.
28. Williams, A. T., Rangel-Buitrago, N., Pranzini, E., & Anfuso, G. (2018). The management of coastal erosion. Ocean & coastal management, 156, 4-20.
29. Wang, C., Wu, Q., Zhang, H., & Liang, F. (2024). Effect of scour remediation by solidified soil on lateral response of monopile supporting offshore wind turbines using numerical model. Applied Ocean Research, 150, 104143.
30. Whitehouse, R. J., Harris, J. M., Sutherland, J., & Rees, J. (2011). The nature of scour development and scour protection at offshore windfarm foundations. Marine Pollution Bulletin, 62(1), 73-88.
31. Chiew, Y. M. (1992). Scour protection at bridge piers. Journal of hydraulic engineering, 118(9), 1260-1269.
32. Pade, C., & Guimaraes, M. (2007). The CO2 uptake of concrete in a 100 year perspective. Cement and concrete research, 37(9), 1348-1356.
33. Chen, Y., Han, Y., Zhang, X., Sarajpoor, S., Zhang, S., & Yao, X. (2023). Experimental study on permeability and strength characteristics of MICP-treated calcareous sand. Biogeotechnics, 1(3), 100034.
34. Peng, S., Di, H., Fan, L., Fan, W., & Qin, L. (2020). Factors affecting permeability reduction of MICP for fractured rock. Frontiers in Earth Science, 8, 217.
35. Song, C., & Elsworth, D. (2024). Stress sensitivity of permeability in high-permeability sandstone sealed with microbially-induced calcium carbonate precipitation. Biogeotechnics, 2(1), 100063.
36. Yu, T., Souli, H., Pechaud, Y., & Fleureau, J. M. (2021). Review on engineering properties of MICP-treated soils. Geomechanics and Engineering, 27(1), 13-30.
37. Lin, H., Suleiman, M. T., & Brown, D. G. (2020). Investigation of pore-scale CaCO3 distributions and their effects on stiffness and permeability of sands treated by microbially induced carbonate precipitation (MICP). Soils and Foundations, 60(4), 944-961.
38. Konstantinou, C., Wang, Y., & Biscontin, G. (2023). A systematic study on the influence of grain characteristics on hydraulic and mechanical performance of MICP-treated porous media. Transport in Porous Media, 147(2), 305-330.
39. Wu, C., Chu, J., Wu, S., & Hong, Y. (2019). 3D characterization of microbially induced carbonate precipitation in rock fracture and the resulted permeability reduction. Engineering Geology, 249, 23-30.
40. Mujah, D., Cheng, L., & Shahin, M. A. (2019). Microstructural and geomechanical study on biocemented sand for optimization of MICP process. Journal of Materials in Civil Engineering, 31(4), 04019025.

 doi:10.20944/preprints202505.1387.v1

41. Liu, S., & Gao, X. (2020). Evaluation of the anti-erosion characteristics of an MICP coating on the surface of tabia. Journal of Materials in Civil Engineering, 32(10), 04020304.
42. Ma, G., He, X., Jiang, X., Liu, H., Chu, J., & Xiao, Y. (2021). Strength and permeability of bentonite-assisted biocemented coarse sand. Canadian Geotechnical Journal, 58(7), 969-981.
43. Sang, G., Lunn, R. J., El Mountassir, G., & Minto, J. M. (2023). Meter-scale MICP improvement of medium graded very gravelly sands: lab measurement, transport modelling, mechanical and microstructural analysis. Engineering Geology, 324, 107275.
44. Yu, X., & Rong, H. (2022). Seawater based MICP cements two/one-phase cemented sand blocks. Applied Ocean Research, 118, 102972.
45. Lin, W., Gao, Y., Lin, W., Zhuo, Z., Wu, W., & Cheng, X. (2023). Seawater-based bio-cementation of natural sea sand via microbially induced carbonate precipitation. Environmental Technology & Innovation, 29, 103010.
46. Boquet, E., Boronat, A., & Ramos-Cormenzana, A. (1973). Production of calcite (calcium carbonate) crystals by soil bacteria is a general phenomenon. Nature, 246(5434), 527-529.
47. Whiffin, V. S. (2004). Microbial CaCO3 precipitation for the production of biocement (Doctoral dissertation, Murdoch University).
48. Mitchell, J. K., & Santamarina, J. C. (2005). Biological considerations in geotechnical engineering. Journal of geotechnical and geoenvironmental engineering, 131(10), 1222-1233.
49. Hosseini, S. M. J., Guan, D., & Cheng, L. (2024). Ground improvement with a single injection of a high-performance all-in-one MICP solution. Geomicrobiology Journal, 41(6), 636-647.
50. Arpajirakul, S., Pungrasmi, W., & Likitlersuang, S. (2021). Efficiency of microbially-induced calcite precipitation in natural clays for ground improvement. Construction and Building Materials, 282, 122722.
51. Wani, K. S., & Mir, B. A. (2022). Application of bio-engineering for marginal soil improvement: an eco-friendly ground improvement technique. Indian Geotechnical Journal, 52(5), 1097-1115.
52. Lin, H., Suleiman, M. T., Jabbour, H. M., Brown, D. G., & Kavazanjian Jr, E. (2016). Enhancing the axial compression response of pervious concrete ground improvement piles using biogrouting. Journal of Geotechnical and Geoenvironmental Engineering, 142(10), 04016045.
53. Lai, H. J., Cui, M. J., & Chu, J. (2023). Effect of pH on soil improvement using one-phase-low-pH MICP or EICP biocementation method. Acta Geotechnica, 18(6), 3259-3272.
54. Zhao, Q., Li, L., Li, C., Li, M., Amini, F., & Zhang, H. (2014). Factors affecting improvement of engineering properties of MICP-treated soil catalyzed by bacteria and urease. Journal of Materials in Civil Engineering, 26(12), 04014094.
55. Karimian, A., & Hassanlourad, M. (2022). Mechanical behaviour of MICP-treated silty sand. Bulletin of Engineering Geology and the Environment, 81(7), 285.
56. Wang, Y. J., Chen, W. B., Li, P. L., Yin, Z. Y., Yin, J. H., & Jiang, N. J. (2024). Soil improvement using biostimulated MICP: Mechanical and biochemical experiments, reactive transport modelling, and parametric analysis. Computers and Geotechnics, 172, 106446.
57. Van Wijngaarden, W. K., Vermolen, F. J., Van Meurs, G. A. M., & Vuik, C. (2011). Modelling biogrout: a new ground improvement method based on microbial-induced carbonate precipitation. Transport in porous media, 87, 397-420.
58. Cheng, L., & Shahin, M. A. (2016). Urease active bioslurry: a novel soil improvement approach based on microbially induced carbonate precipitation. Canadian Geotechnical Journal, 53(9), 1376-1385.
59. Wang, Y., Konstantinou, C., Soga, K., Biscontin, G., & Kabla, A. J. (2022). Use of microfluidic experiments to optimize MICP treatment protocols for effective strength enhancement of MICP-treated sandy soils. Acta Geotechnica, 17(9), 3817-3838.
60. Teng, F., Sie, Y. C., & Ouedraogo, C. (2021). Strength improvement in silty clay by microbial-induced calcite precipitation. Bulletin of Engineering Geology and the Environment, 80(8), 6359-6371.
61. Chae, S. H., Chung, H., & Nam, K. (2021). Evaluation of microbially Induced calcite precipitation (MICP) methods on different soil types for wind erosion control. Environmental Engineering Research, 26(1).

 doi:10.20944/preprints202505.1387.v1

62. Wang, Y. N., Li, S. K., Li, Z. Y., & Garg, A. (2023). Exploring the application of the MICP technique for the suppression of erosion in granite residual soil in Shantou using a rainfall erosion simulator. Acta Geotechnica, 18(6), 3273-3285.
63. Wang, Z., Zhang, N., Jin, Y., Li, Q., & Xu, J. (2021). Application of microbially induced calcium carbonate precipitation (MICP) in sand embankments for scouring/erosion control. Marine Georesources & Geotechnology, 39(12), 1459-1471.
64. Liu, S., & Gao, X. (2020a). Evaluation of the anti-erosion characteristics of an MICP coating on the surface of tabia. Journal of Materials in Civil Engineering, 32(10), 04020304.
65. Liu, S., Wang, R., Yu, J., Peng, X., Cai, Y., & Tu, B. (2020b). Effectiveness of the anti-erosion of an MICP coating on the surfaces of ancient clay roof tiles. Construction and Building Materials, 243, 118202.
66. Liu, S., Du, K., Huang, W., Wen, K., Amini, F., & Li, L. (2021). Improvement of erosion-resistance of bio-bricks through fiber and multiple MICP treatments. Construction and Building Materials, 271, 121573.
67. Jiang, N. J., Soga, K., & Kuo, M. (2017). Microbially induced carbonate precipitation for seepage-induced internal erosion control in sand–clay mixtures. Journal of Geotechnical and Geoenvironmental Engineering, 143(3), 04016100.
68. Jiang, N. J., & Soga, K. (2019). Erosional behavior of gravel-sand mixtures stabilized by microbially induced calcite precipitation (MICP). Soils and Foundations, 59(3), 699-709.
69. Chek, A., Crowley, R., Ellis, T. N., Durnin, M., & Wingender, B. (2021). Evaluation of factors affecting erodibility improvement for MICP-treated beach sand. Journal of Geotechnical and Geoenvironmental Engineering, 147(3), 04021001.
70. Li, K., & Wang, Y. (2024). The impact of Microbially Induced Calcite Precipitation (MICP) on sand internal erosion resistance: A microfluidic study. Transportation Geotechnics, 49, 101404.
71. Meng, H., Gao, Y., He, J., Qi, Y., & Hang, L. (2021). Microbially induced carbonate precipitation for wind erosion control of desert soil: Field-scale tests. Geoderma, 383, 114723.
72. Cheng, Y. J., Tang, C. S., Pan, X. H., Liu, B., Xie, Y. H., Cheng, Q., & Shi, B. (2021). Application of microbial induced carbonate precipitation for loess surface erosion control. Engineering Geology, 294, 106387.
73. Zhang, Z., Lu, H., Tang, X., Liu, K., Ye, L., & Ma, G. (2024). Field investigation of the feasibility of MICP for Mitigating Natural Rainfall-Induced erosion in gravelly clay slope. Bulletin of Engineering Geology and the Environment, 83(10), 406.
74. Xiao, Y., Ma, G., Wu, H., Lu, H., & Zaman, M. (2022). Rainfall-induced erosion of biocemented graded slopes. International Journal of Geomechanics, 22(1), 04021256.
75. Liu, B., Tang, C. S., Pan, X. H., Cheng, Q., Xu, J. J., & Lv, C. (2025). Mitigating rainfall induced soil erosion through bio-approach: From laboratory test to field trail. Engineering Geology, 344, 107842.
76. Sun, X., Miao, L., Wang, H., Wu, L., Fan, G., & Xia, J. (2022). Sand foreshore slope stability and erosion mitigation based on microbiota and enzyme mix–induced carbonate precipitation. Journal of Geotechnical and Geoenvironmental Engineering, 148(8), 04022058.
77. Rodríguez, R. F., & Cardoso, R. (2022). Study of biocementation treatment to prevent erosion by concentrated water flow in a small-scale sand slope. Transportation Geotechnics, 37, 100873.
78. Jongvivatsakul, P., Janprasit, K., Nuaklong, P., Pungrasmi, W., & Likitlersuang, S. (2019). Investigation of the crack healing performance in mortar using microbially induced calcium carbonate precipitation (MICP) method. Construction and Building Materials, 212, 737-744.
79. Sun, X., Miao, L., Wu, L., & Wang, H. (2021). Theoretical quantification for cracks repair based on microbially induced carbonate precipitation (MICP) method. Cement and Concrete Composites, 118, 103950.
80. Choi, S. G., Wang, K., Wen, Z., & Chu, J. (2017). Mortar crack repair using microbial induced calcite precipitation method. Cement and Concrete Composites, 83, 209-221.
81. Intarasoontron, J., Pungrasmi, W., Nuaklong, P., Jongvivatsakul, P., & Likitlersuang, S. (2021). Comparing performances of MICP bacterial vegetative cell and microencapsulated bacterial spore methods on concrete crack healing. Construction and Building Materials, 302, 124227.

 doi:10.20944/preprints202505.1387.v1

82. Nuaklong, P., Jongvivatsakul, P., Phanupornprapong, V., Intarasoontron, J., Shahzadi, H., Pungrasmi, W., ... & Likitlersuang, S. (2023). Self-repairing of shrinkage crack in mortar containing microencapsulated bacterial spores. Journal of Materials Research and Technology, 23, 3441-3454.
83. Jiang, L., Xia, H., Hu, S., Zhao, X., Wang, W., Zhang, Y., & Li, Z. (2024). Crack-healing ability of concrete enhanced by aerobic-anaerobic bacteria and fibers. Cement and Concrete Research, 183, 107585.
84. Zamani, A., Xiao, P., Baumer, T., Carey, T. J., Sawyer, B., DeJong, J. T., & Boulanger, R. W. (2021). Mitigation of liquefaction triggering and foundation settlement by MICP treatment. Journal of Geotechnical and Geoenvironmental Engineering, 147(10), 04021099.
85. O'Donnell, S. T., Kavazanjian Jr, E., & Rittmann, B. E. (2017a). MIDP: Liquefaction mitigation via microbial denitrification as a two-stage process. II: MICP. Journal of Geotechnical and Geoenvironmental Engineering, 143(12), 04017095.
86. O'Donnell, S. T., Rittmann, B. E., & Kavazanjian Jr, E. (2017b). MIDP: Liquefaction mitigation via microbial denitrification as a two-stage process. I: Desaturation. Journal of Geotechnical and Geoenvironmental Engineering, 143(12), 04017094.
87. Han, Z., Zhang, J., Bian, H., Yue, J., Xiao, J., & Wei, Y. (2024). Study on Liquefaction-Resistance Performance of MICP-Cemented Sands: Applying Centrifuge Shake Table Tests. Journal of Geotechnical and Geoenvironmental Engineering, 150(8), 06024004.
88. Ahenkorah, I., Rahman, M. M., Karim, M. R., & Beecham, S. (2024). Cyclic liquefaction resistance of MICP- and EICP-treated sand in simple shear conditions: A benchmarking with the critical state of untreated sand. Acta Geotechnica, 19(9), 5891-5913.
89. Xiao, P., Liu, H., Xiao, Y., Stuedlein, A. W., & Evans, T. M. (2018). Liquefaction resistance of bio-cemented calcareous sand. Soil Dynamics and Earthquake Engineering, 107, 9-19.
90. Xiao, Y., Zhang, Z., Stuedlein, A. W., & Evans, T. M. (2021). Liquefaction modeling for biocemented calcareous sand. Journal of Geotechnical and Geoenvironmental Engineering, 147(12), 04021149.
91. Zhou, Y., Zhang, Y., Geng, W., He, J., & Gao, Y. (2023). Evaluation of liquefaction resistance for single-and multi-phase SICP-treated sandy soil using shaking table test. Acta Geotechnica, 18(11), 6007-6025.
92. Zhang, X., Chen, Y., Liu, H., Zhang, Z., & Ding, X. (2020). Performance evaluation of a MICP-treated calcareous sandy foundation using shake table tests. Soil Dynamics and Earthquake Engineering, 129, 105959.
93. Darby, K. M., Hernandez, G. L., DeJong, J. T., Boulanger, R. W., Gomez, M. G., & Wilson, D. W. (2019). Centrifuge model testing of liquefaction mitigation via microbially induced calcite precipitation. Journal of Geotechnical and Geoenvironmental Engineering, 145(10), 04019084.
94. Kanwal, M., Khushnood, R. A., Adnan, F., Wattoo, A. G., & Jalil, A. (2023). Assessment of the MICP potential and corrosion inhibition of steel bars by biofilm forming bacteria in corrosive environment. Cement and Concrete Composites, 137, 104937.
95. Sun, X., Wai, O. W., Xie, J., & Li, X. (2023). Biomineralization to prevent microbially induced corrosion on concrete for sustainable marine infrastructure. Environmental science & technology, 58(1), 522-533.
96. Umar, M., Kassim, K. A., & Chiet, K. T. P. (2016). Biological process of soil improvement in civil engineering: A review. Journal of Rock Mechanics and Geotechnical Engineering, 8(5), 767-774.
97. Rajasekar, A., Wilkinson, S., & Moy, C. K. (2021). MICP as a potential sustainable technique to treat or entrap contaminants in the natural environment: A review. Environmental Science and Ecotechnology, 6, 100096.
98. Mujah, D., Shahin, M. A., & Cheng, L. (2017). State-of-the-art review of biocementation by microbially induced calcite precipitation (MICP) for soil stabilization. Geomicrobiology Journal, 34(6), 524-537.
99. Zhang, K., Tang, C. S., Jiang, N. J., Pan, X. H., Liu, B., Wang, Y. J., & Shi, B. (2023). Microbial-induced carbonate precipitation (MICP) technology: a review on the fundamentals and engineering applications. Environmental Earth Sciences, 82(9), 229.
100. Fu, T., Saracho, A. C., & Haigh, S. K. (2023). Microbially induced carbonate precipitation (MICP) for soil strengthening: A comprehensive review. Biogeotechnics, 1(1), 100002.

 doi:10.20944/preprints202505.1387.v1

101. Wang, Z., Zhang, N., Cai, G., Jin, Y., Ding, N., & Shen, D. (2017). Review of ground improvement using microbial induced carbonate precipitation (MICP). Marine Georesources & Geotechnology, 35(8), 1135-1146.
102. Gebru, K. A., Kidanemariam, T. G., & Gebretinsae, H. K. (2021). Bio-cement production using microbially induced calcite precipitation (MICP) method: A review. Chemical Engineering Science, 238, 116610.
103. Fouladi, A. S., Arulrajah, A., Chu, J., & Horpibulsuk, S. (2023). Application of Microbially Induced Calcite Precipitation (MICP) technology in construction materials: A comprehensive review of waste stream contributions. Construction and Building Materials, 388, 131546.
104. Wang, Y., Sun, X., Miao, L., Wang, H., Wu, L., Shi, W., & Kawasaki, S. (2024). State-of-the-art review of soil erosion control by MICP and EICP techniques: Problems, applications, and prospects. Science of the Total Environment, 912, 169016.
105. Kumar, A., Song, H. W., Mishra, S., Zhang, W., Zhang, Y. L., Zhang, Q. R., & Yu, Z. G. (2023). Application of microbial-induced carbonate precipitation (MICP) techniques to remove heavy metal in the natural environment: A critical review. Chemosphere, 318, 137894.
106. Harran, R., Terzis, D., & Laloui, L. (2023). Mechanics, modeling, and upscaling of biocemented soils: a review of breakthroughs and challenges. International Journal of Geomechanics, 23(9), 03123004.
107. DeJong, J. T., Mortensen, B. M., Martinez, B. C., & Nelson, D. C. (2010). Bio-mediated soil improvement. Ecological engineering, 36(2), 197-210.
108. Wu, H., Wu, W., Liang, W., Dai, F., Liu, H., & Xiao, Y. (2023). 3D DEM modeling of biocemented sand with fines as cementing agents. International Journal for Numerical and Analytical Methods in Geomechanics, 47(2), 212-240.
109. Stocks-Fischer, S., Galinat, J. K., & Bang, S. S. (1999). Microbiological precipitation of CaCO3. Soil biology and biochemistry, 31(11), 1563-1571.
110. Lin, W., Gao, Y., Lin, W., Zhuo, Z., Wu, W., & Cheng, X. (2023). Seawater-based bio-cementation of natural sea sand via microbially induced carbonate precipitation. Environmental Technology & Innovation, 29, 103010.
111. Silva-Castro, G. A., Uad, I., Rivadeneyra, A., Vilchez, J. I., Martin-Ramos, D., González-López, J., & Rivadeneyra, M. A. (2013). Carbonate precipitation of bacterial strains isolated from sediments and seawater: formation mechanisms. Geomicrobiology Journal, 30(9), 840-850.
112. Kang, B., Wang, H., Zha, F., Liu, C., Zhou, A., & Ban, R. (2025). Exploring the Uniformity of MICP Solidified Fine Particle Silt with Different Sample Preparation Methods. Biogeotechnics, 100163.
113. Zhu, Y. Q., Li, Y. J., Sun, X. Y., Guo, Z., Rui, S. J., & Zheng, D. Q. (2025). A one-phase injection method to improve the strength and uniformity in MICP with polycarboxylic acid added. Acta Geotechnica, 1-13.
114. Clarà Saracho, A., Haigh, S. K., & Ehsan Jorat, M. (2021). Flume study on the effects of microbial induced calcium carbonate precipitation (MICP) on the erosional behaviour of fine sand. Géotechnique, 71(12), 1135-1149.
115. Salifu, E., MacLachlan, E., Iyer, K. R., Knapp, C. W., & Tarantino, A. (2016). Application of microbially induced calcite precipitation in erosion mitigation and stabilisation of sandy soil foreshore slopes: A preliminary investigation. Engineering Geology, 201, 96-105.
116. Kou, H. L., Wu, C. Z., Ni, P. P., & Jang, B. A. (2020). Assessment of erosion resistance of biocemented sandy slope subjected to wave actions. Applied Ocean Research, 105, 102401.
117. Li, Y., Xu, Q., Li, Y., Li, Y., & Liu, C. (2022a). Application of microbial-induced calcium carbonate precipitation in wave erosion protection of the sandy slope: An experimental study. Sustainability, 14(20), 12965.
118. Ghasemi, P., & Montoya, B. M. (2022). Field implementation of microbially induced calcium carbonate precipitation for surface erosion reduction of a coastal plain sandy slope. Journal of Geotechnical and Geoenvironmental Engineering, 148(9), 04022071.
119. Li, Y., Guo, Z., Wang, L., Zhu, Y., & Rui, S. (2024). Field implementation to resist coastal erosion of sandy slope by eco-friendly methods. Coastal Engineering, 189, 104489.
120. Li, Y., Guo, Z., Wang, L., Yang, H., Li, Y., & Zhu, J. (2022b). An innovative eco-friendly method for scour protection around monopile foundation. Applied Ocean Research, 123, 103177.

 doi:10.20944/preprints202505.1387.v1

121. Zhu, T., He, R., Hosseini, S. M. J., He, S., Cheng, L., Guo, Y., & Guo, Z. (2024). Influence of precast microbial reinforcement on lateral responses of monopiles. Ocean Engineering, 307, 118211.
122. Wang, X., Tao, J., Bao, R., Tran, T., & Tucker-Kulesza, S. (2018). Surficial soil stabilization against water-induced erosion using polymer-modified microbially induced carbonate precipitation. Journal of Materials in Civil Engineering, 30(10), 04018267.
123. Martinez, B. C., DeJong, J. T., & Ginn, T. R. (2014). Bio-geochemical reactive transport modeling of microbial induced calcite precipitation to predict the treatment of sand in one-dimensional flow. Computers and Geotechnics, 58, 1-13.
124. Fauriel, S., & Laloui, L. (2012). A bio-chemo-hydro-mechanical model for microbially induced calcite precipitation in soils. Computers and Geotechnics, 46, 104-120.
125. Wang, X., & Nackenhorst, U. (2020). A coupled bio-chemo-hydraulic model to predict porosity and permeability reduction during microbially induced calcite precipitation. Advances in Water Resources, 140, 103563.
126. Bosch, J. A., Terzis, D., & Laloui, L. (2024). A bio-chemo-hydro-mechanical model of transport, strength and deformation for bio-cementation applications. Acta Geotechnica, 19(5), 2805-2821.
127. Koponen A., Kataja M., Timonen J. (1997). Permeability and effective porosity of porous media. Physical review E, 56(3):3319-3325.
128. Li, Y., Guo, Z., Wang, L., & Yang, H. (2023). A coupled bio-chemo-hydro-wave model and multi-stages for MICP in the seabed. Ocean Engineering, 280, 114667.
129. Li, Y., Wang, L., Dong, C., et al. (2025). A coupled mathematical model of microbial grouting reinforced seabed considering the response of wave-induced pore pressure and its application. Computers and Geotechnics, 184, 107235.
130. Yamamoto T., Koning H., Sellmeijer H. (1978). “On the response of a poroelastic bed to water waves.” Journal of Fluid Mechanics, 78:193-206.